Clinical-imaging-radiomic nomogram based on unenhanced CT effectively predicts adrenal metastases in patients with lung cancer with small hyperattenuating adrenal incidentalomas

LIXIU CAO[1*], HAOXUAN YANG[2*], DESHUN YAO[3*], HAIFENG CAI[3], HUIJING WU[1], YIXING YU[4], LEI ZHU[5], WENGUI XU[5], YONGLIANG LIU[6] and JINGWU LI[7]

[1]Department of Nuclear Medical Imaging, Tangshan People's Hospital, Tangshan, Hebei 063000, P.R. China; [2]Department of Urology, The Second Hospital of Hebei Medical University, Shijiazhuang, Hebei 050010, P.R. China; [3]Department of Oncology Surgery, Tangshan People's Hospital, Tangshan, Hebei 063000, P.R. China; [4]Department of Radiology, The First Affiliated Hospital of Soochow University, Suzhou, Jiangsu 215006, P.R. China; [5]Department of Molecular Imaging and Nuclear Medicine, Tianjin Medical University Cancer Institute and Hospital, National Clinical Research Center for Cancer, Tianjin Key Laboratory of Cancer Prevention and Therapy, Tianjin's Clinical Research Center for Cancer, Tianjin 300000, P.R. China; [6]Department of Neurosurgery, Tangshan People's Hospital, Tangshan, Hebei 063000, P.R. China; [7]Department of Tumor Surgery, Tangshan People's Hospital, Tangshan, Hebei 063000, P.R. China

Received October 18, 2023; Accepted April 26, 2024

DOI: 10.3892/ol.2024.14472

Abstract. The aim of the present study was to develop and evaluate a clinical-imaging-radiomic nomogram based on pre-enhanced computed tomography (CT) for pre-operative differentiation lipid-poor adenomas (LPAs) from metastases in patients with lung cancer with small hyperattenuating adrenal incidentalomas (AIs). A total of 196 consecutive patients with lung cancer, who underwent initial chest or abdominal pre-enhanced CT scan with small hyperattenuating AIs, were included. The patients were randomly divided into a training cohort with 71 cases of LPAs and 66 cases of metastases, and a testing cohort with 31 cases of LPAs and 28 cases of metastases. Plain CT radiological and clinical features were evaluated, including sex, age, size, pre-enhanced CT value (CT_{pre}), shape, homogeneity and border. A total of 1,316 radiomic features were extracted from the plain CT images of the AIs, and the significant features selected by the least absolute shrinkage and selection operator were used to establish a Radscore. Subsequently, a clinical-imaging-radiomic model was developed by multivariable logistic regression incorporating the Radscore with significant clinical and imaging features. This model was then presented as a nomogram. The performance of the nomogram was assessed by calibration curves and decision curve analysis (DCA). A total of 4 significant radiomic features were incorporated in the Radscore, which yielded notable area under the receiver operating characteristic curves (AUCs) of 0.920 in the training dataset and 0.888 in the testing dataset. The clinical-imaging-radiomic nomogram incorporating the Radscore, CT_{pre}, sex and age revealed favourable differential diagnostic performance (AUC: Training, 0.968; testing, 0.915) and favourable calibration curves. The nomogram was revealed to be more useful than the Radscore and the clinical-imaging model in clinical practice by DCA. The clinical-imaging-radiomics nomogram based on initial plain CT images by integrating the Radscore and clinical-imaging factors provided a potential tool to effectively differentiate LPAs from metastases in patients with lung cancer with small hyperattenuating AIs.

Correspondence to: Dr Jingwu Li, Department of Tumor Surgery, Tangshan People's Hospital, 65 Shengli Road, Lunan, Tangshan, Hebei 063000, P.R. China
E-mail: tslijingwu@163.com

Mr. Yongliang Liu, Department of Neurosurgery, Tangshan People's Hospital, 65 Shengli Road, Lunan, Tangshan, Hebei 063000, P.R. China
E-mail: langqy09@126.com

*Contributed equally

Abbreviations: LPA, lipid-poor adenoma; AI, adrenal incidentaloma; LASSO, least absolute shrinkage and selection operator; AUC, area under the receiver operating characteristic curve; DCA, decision curve analysis; LD, long diameter; SD, short diameter; CT_{pre}, pre-enhanced CT value; VOI, volume of interest; CI, confidence interval; ICC, intra-class correlation coefficient; HU, Hounsfield units; OR, odds ratio

Key words: AI, unenhanced CT, radiomic nomogram, Radscore, LPA, metastases

Introduction

Adrenal incidentalomas (AIs) are frequently observed during clinical investigation and the detection rate is increasing

with the increasing role of CT, MRI and PET in diagnosing, staging, and follow-up of malignancies (1,2). Among AIs, 70-80% are adenomas and only ~5% are metastases, but the risk of metastases increases substantially in patients with a history of lung cancer. Numerous patients with lung cancer at the time of diagnosis present with distant metastases, with the adrenal gland the frequent site of metastatic spread (3,4). In a number of cases, a specific diagnosis of AIs can be established through a combination of endocrine function tests, clinical symptom assessment and radiological analysis. However, in patients with a history of lung cancer and non-functioning AIs, radiologic characteristics play an important role in evaluating those patients (5,6). Furthermore, when a small AI [long diameter (LD) ≤4 cm] with pre-enhanced CT value (CT_{pre}) ≥10 Hounsfield units (HU) is detected at the initial chest or abdominal plain CT scan, immediate differentiation between metastases and lipid-poor adenomas (LPAs) can be challenging due to overlapping imaging features (7-9). As a result, additional confirmatory steps, such as adrenal washout CT, chemical-shift MRI, PET/CT scans or biopsies, may be required for an accurate diagnosis (10-14).

Although the use of adrenal washout CT for characterizing LPAs has demonstrated relatively high sensitivity and specificity (15), several drawbacks warrant consideration, such as radiation hazards, additional cost and the potential risks associated with contrast media, including potential renal damage and allergic reactions. In addition, in vulnerable populations such as patients with diabetes or renal insufficiency, and the elderly and paediatric populations, the potential risks may be further exacerbated. Chemical-shift MRI, which is the most sensitive examination method, still leaves a portion of LPAs (~10-20%) as indeterminate. Additionally, not all patients have high-quality MRI images, and some patients have contraindications for MRI examination (16,17). As for PET/CT scans, there is a certain overlap in fluorodeoxyglucose uptake between metastases and adenomas (18). Moreover, PET/CT is not commonly available in a number of medical institutions, and thus results in greater financial and time costs for the patient. Adrenal biopsy, as an invasive test, may lead to some complications (19).

Therefore, it would be of great significance if the images could provide more valuable information to help identify LPAs from metastases in patients with lung cancer on the initial discovery examination, which is usually a chest or abdominal plain CT scan, especially for patients with diabetes or renal insufficiency.

Radiomics can extract larger numbers of objective and quantitative image-related features from CT images. These features encompass texture, geometry and intensity, offering insights into tumor heterogeneity and enabling the exploration of potential correlations between pathophysiology and biomedical images (20,21). A combined radiomic model incorporating radiomic features with relevant clinical and imaging features, as a complex bioinformatics mining tool, may improve the accuracy of differential diagnosis, classification and prediction (22,23). However, the specific effectiveness of the Radscore and the combined radiomic model based on unenhanced CT in differentiating LPAs from metastases in patients with lung cancer is not known.

Thus, the present retrospective study attempts to develop and validate a clinical-imaging-radiomic nomogram combining the Radscore with significant clinical-imaging features based on initial unenhanced CT to differentiate LPAs from metastases in patients with lung cancer with small hyperattenuating AIs.

Materials and methods

Patients. The present study received approval (approval no. RMYY-LLKS-2023202) from Tangshan People's Hospital Institutional Ethics Committee (Tangshan, China). Written informed consent was obtained from all patients regarding the use and publication of their existing clinical-pathological-CT data. Patients with a history of histopathological verification of lung cancer before or after undergoing chest or abdominal plain CT scan with diagnostic indications such as 'adrenal metastasis' or 'adrenal adenoma' or 'adrenal nodule or mass' from January 2014 to March 2022 were included at Tangshan People's hospital (Tangshan, China). Inclusion criteria were as follows: i) CT_{pre} ≥10 HU and small unilateral lesions; ii) non-functioning adrenal tumor; and iii) availability of complete imaging and clinical data. The eligibility criteria for diagnosing adrenal metastases were as follows: i) Histological confirmation through needle biopsy or resection specimen (n=2); ii) interval development of an adrenal mass compared with a previous CT scan showing a normal adrenal gland (n=63); and iii) short-term interval growth [a 20% reduce or increase in the total sum of the disease within six months (24)] in the same patient (n=29). The eligibility criteria for diagnosing LPAs were as follows: i) Surgical excision with subsequent histopathological assessment (n=81); and ii) stability in size after at least 1-year interval (mean follow-up time, 738±601 days; n=21) (25).

The present study included a total of 196 patients with adrenal lesions, consisting of 94 metastases and 102 LPAs. The patients were randomly divided into a training cohort (n=137, comprising 66 metastases and 71 LPAs) and a testing cohort (n=59, comprising 28 metastases and 31 LPAs) using a random seed method at a ratio of 7:3 (Fig. 1).

Images protocol. Given the retrospective nature of the present study, multiple CT scanners were employed, including the Brilliance 16 and Ingenuity core 64 (Philips Healthcare) and the GE Discovery CT 750 HD (Cytiva). All patients underwent chest or abdominal plain CT scans, with the following scanning parameters: 120 Kv, automatic tube current of 200-300 mA, 2 or 5-mm slice thickness, and then 5 mm images were reconstructed with a section thickness of 1.25 or 2 mm.

Imaging features. The LD, short diameter (SD), shape, laterality (right or left), border, homogeneity, CT_{pre} and calcification of AIs were independently measured and assessed by two radiologists who possessed 6 and 10 years of experience in diagnosing abdominal CT images using thin-sliced plain CT scans. The LD and SD measurements were taken at the maximum cross-section of the AIs. A region of interest covering two-thirds of the maximum axial area of the nodule was delineated, ensuring exclusion of adjacent fat. In some cases, their results were consistent

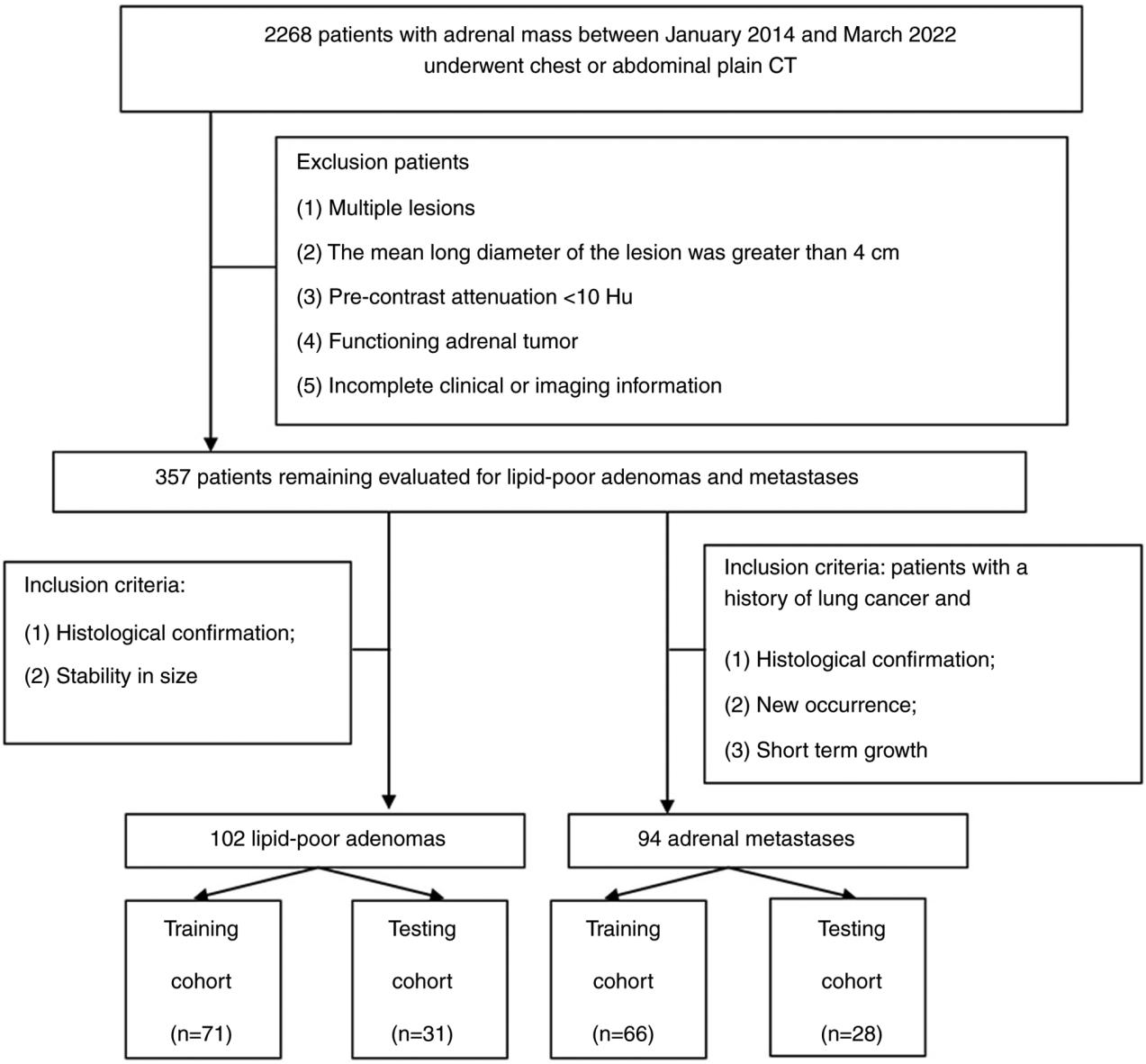

Figure 1. Flowchart illustrates the patient selection process, along with the criteria for inclusion and exclusion.

and their results were directly used in subsequent analyses; When there was a disagreement, a consensus was reached through discussion (26).

Radiomics feature extraction, selection and Radscore building. A total of two abdominal radiologists, each with 4 and 6 years of experience using the 3D Slicer software (version 4.13.0; National Institutes of Health), manually delineated volumes of interest (VOIs) for the AIs. Great care was taken to encompass as much of the lesion as possible while meticulously avoiding the inclusion of external structures (Fig. 2A) (27). The reproducibility of VOIs delineated by both radiologists was evaluated, and those delineated by the radiologist with 6 years of experience were chosen for subsequent radiomics analysis (Fig. 2B). Radiomics' features were extracted using Slicer Radiomics (version 1.0.0; Artificial Intelligence in Medicine Program), an extension that utilized SuperBuild to create a separate library, pyradiomics (version 3.0; Artificial Intelligence in Medicine Program) and a dependent scripted Module. These features were computed on both original or pre-processed images, employing Laplacian of Gaussian filters with varying σ values (1.0, 2.0, 3.0, 4.0, 5.0) and wavelets. The calculation was performed with an intensity bin width of 25 and resampled voxel dimensions of 1x1x1 mm^3. The extracted radiomics features included first-order statistics, shape characteristics and texture features. Texture features encompassed gray level dependence matrix, gray level co-occurrence matrix, neighbouring gray tone difference matrix, gray level size zone matrix and gray level run length matrix. The least absolute shrinkage and selection operator (LASSO) method, renowned for its capability to reduce dimensionality and redundancy, was employed for feature selection in the training dataset (Fig. 2C). The optimal value of the penalization parameter λ was identified through a five-fold cross-validation process. Subsequently, the optimal features were determined by adjusting λ to correspond to one standard error of the minimum loss (Fig. 2D).

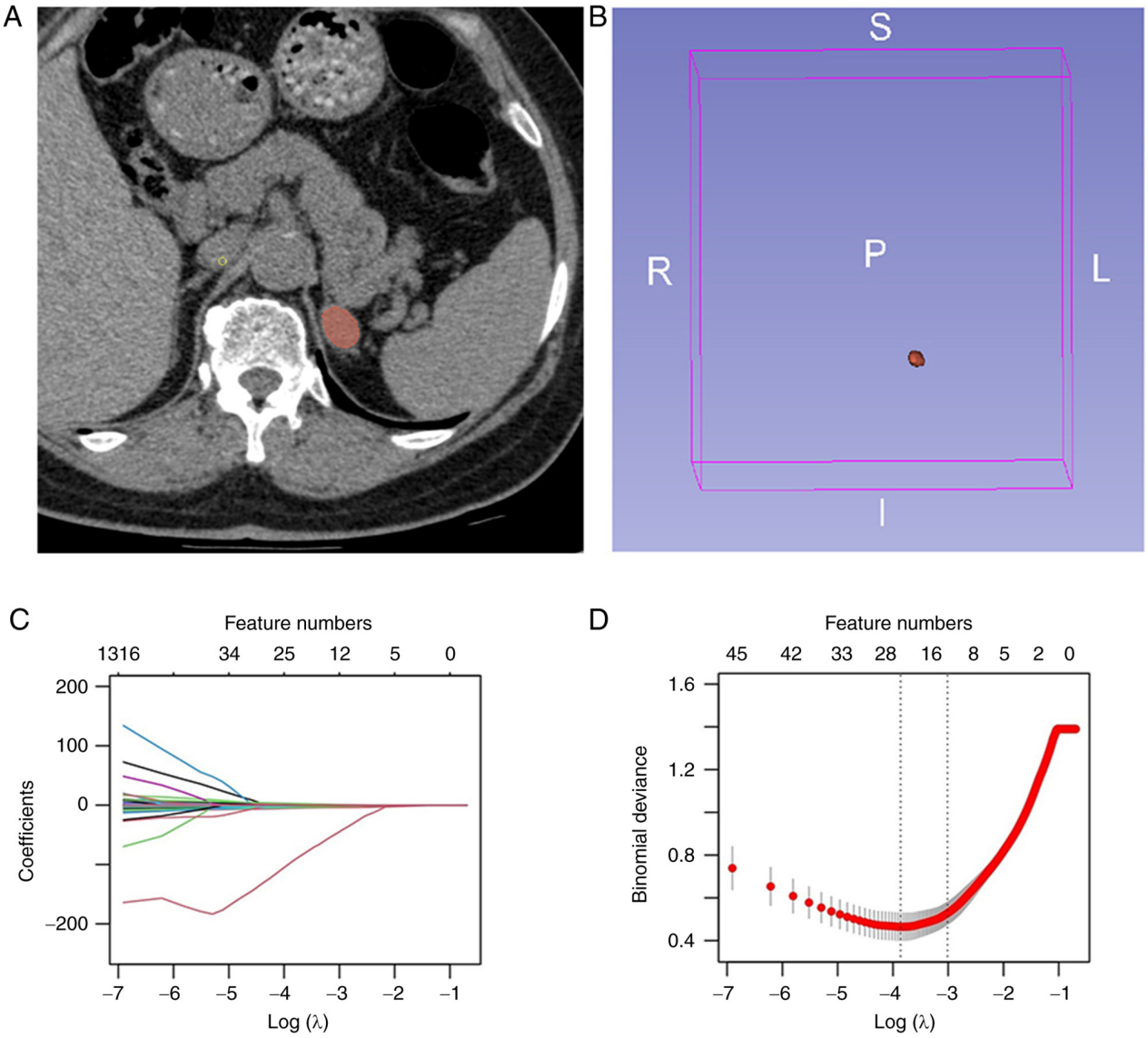

Figure 2. Delineation of VOI and selection of radiomic features. (A) Delineation of the intratumoral region in the unenhanced computed tomography images. (B) Three-dimensional VOI of adrenal mass. (C) LASSO coefficient profiles (y-axis) of the radiomics features. The lower x-axis indicated the logλ. The top x-axis has the average number of predictors. (D) A total of 13 radiomics features were selected into the LASSO model by adjusting λ to one standard error of the minimum loss (the dashed line on right). The dashed line on left represented adjusting λ to the minimum loss. VOI, volume of interest; LASSO, least absolute shrinkage and selection operator.

After deleting the high correlation coefficient (>0.7), the remaining useful features were employed in constructing the Radscore using a multivariable logistic regression formula: Radscore=1/[1+eʌ(-β0-β1xX1-β2xX2-…-βmxXm)].

Diagnostic validation of Radscore and significant clinical and imaging features. The potential diagnostic performance of the Radscore, and the significant clinical and imaging features for differentiating metastases from LPAs were assessed using the area under the receiver operating characteristic (ROC) curves (AUCs), and the optimal cut-off values for maximum specificity and sensitivity were determined using the Youden index.

Development and validation of the clinical-imaging-radiomic model and nomogram. The risk factors for diagnosis of metastases were selected by stepwise binary logistic regression based on a likelihood test. Subsequently, the final risk factors were introduced in the multiple logistic regression to establish the clinical-imaging-radiomic model in the training cohort. The performance of this model was evaluated by AUC in both the training and testing datasets. To further evaluate the diagnostic ability of the nomogram developed from the clinical-imaging-radiomic model, a decision curve analysis (DCA) and calibration curve were employed.

Development and validation of the clinical-imaging model. Sex, age, CT_{pre} and shape were significant differences in the training and testing datasets between LPAs and metastases by the chi-square test or independent-sample t-test. Three variables including sex, age and CT_{pre} selected by multivariate logistic regression were independent factors for differentiating metastases from LPAs in patients with lung cancer. Then, the final risk factors were incorporated in the multivariate logistic

Table I. Clinical-imaging characteristics and rad-score of patients in the training and testing cohorts.

	Training cohort (n=137)				Testing cohort (n=59)				
Characteristic	Total (n=137)	LPAs (n=71)	Metastases (n=66)	P value	Total (n=59)	LPAs (n=31)	Metastases (n=28)	P-value	P^{Δ}value
Sex				<0.0001[a]				0.001[a]	0.448
Male	80 (58.39%)	30 (42.25%)	50 (75.76%)		31 (52.54%)	10 (32.26%)	21 (75%)		
Female	57 (41.61%)	41 (57.75%)	16 (24.24%)		28 (47.46%)	21 (67.74%)	7 (25%)		
Age, (years)	58.96±9.87	56.10±11.08	62.05±7.27	<0.0001[a]	58.73±11.65	55.42±12.94	62.39±8.88	0.020[a]	0.885
Long diameter (mm)	19.86±7.52	19.92±7.01	19.81±8.09	0.934	20.10±8.79	20.61±9.32	20.17±8.35	0.849	0.662
Short diameter (mm)	15.84±5.99	15.93±5.49	15.74±6.52	0.852	16.63±7.32	17.39±7.87	15.78±6.69	0.405	0.431
Lesion location				0.117				0.098	0.629
Right	53 (38.69%)	23 (32.39%)	30 (45.45%)		25 (42.37%)	10 (32.26%)	15 (53.57%)		
Left	84 (61.31%)	48 (67.61%)	36 (54.55%)		34 (57.63%)	21 (67.74%)	13 (46.43%)		
CT_{pre} (Hu)	32.72±10.72	26.30±8.48	39.62±8.35	<0.001[a]	32.86±10.72	29.35±11.91	36.75±7.71	0.006[a]	0.929
Shape				0.003[a]				0.024[a]	0.187
Regular	123 (89.78%)	69 (97.18%)	54 (81.82%)		49 (83.05%)	29 (93.55%)	20 (71.43%)		
Irregular	14 (10.21%)	2 (2.82%)	12 (18.18%)		10 (16.95%)	2 (6.45%)	8 (28.57%)		
Homogeneity				0.773				0.338	0.268
Homogenous	130 (94.89%)	67 (64.37%)	63 (95.45%)		58 (98.31%)	30 (96.77%)	28 (100%)		
Heterogenous	7 (5.11%)	4 (5.63%)	3 (4.55%)		1 (1.69%)	1 (3.23%)	0 (0%)		
Border				0.140				0.289	0.902
Sharp	135 (98.54%)	71 (100%)	64 (96.97%)		58 (98.31%)	31 (100%)	27 (96.43%)		
Blotted	2 (1.46%)	0 (0%)	2 (3.03%%)		1 (1.69%)	0 (0%)	1 (3.57%)		
Calcification				0.517				0.130	0.625
Yes	3 (2.19%)	1 (1.41%)	2 (3.03%)		2 (3.39%)	0(0%)	2 (7.14%)		
No	134 (97.81%)	70 (98.59%)	64 (96.97%)		57 (96.61%)	31 (100%)	26 (92.86%)		
Radscore	0.48±0.37	0.22±0.24	0.76±0.27	<0.0001[a]	0.45±0.36	0.23±0.24	0.70±0.30	0.0001[a]	0.593

[a]P<0.05 indicates a significant difference between LPAs and metastases in the training or validation cohort; P^{Δ}<0.05 indicates a significant difference between the training and validation cohorts. LPAs, lipid-poor adenomas; CT, computed tomography; Hu, Hounsfield units; CT_{pre}, pre-enhanced CT value.

regression to construct the clinical-imaging model in the training cohort. AUC analysis was used to quantify the predictive performance of clinical-imaging model in the training dataset and test the predictive performance in the testing dataset, respectively (Fig. S1).

Statistical analysis. R software (version 4.1.2; The R Foundation) and IBM SPSS Statistics software (version 21; IBM Corp.) were used for statistical analyses. Quantitative parameters and categorical variables were compared using the Mann-Whitney U test or independent-sample t-test and chi-square test, respectively. The inter-observer reproducibility of feature extraction was evaluated using the intra-class correlation coefficient (ICC). An ICC value <0.5 indicated low consistency, while values between 0.5 and 0.79 were considered medium, and values ≥0.8 indicated high consistency.

The LASSO regression was implemented using the 'glmnet' package in R software, the 'corrplot' package was used to calculate the correlation between variables, logistic regression and nomogram were implemented by the 'rms' package, and DCA was implemented by the 'rmda' package. P<0.05 was considered to indicate a statistically significant difference.

Results

Clinical and imaging characteristics. Patient characteristics, including sex, age, LD, SD, location, CT_{pre}, shape, border, homogeneity, calcification and Radscore, showed no significant differences between the training and testing datasets (Table I; P>0.05), indicating that it was reasonable to randomly partition the complete dataset by random seeds. However, sex, age, CT_{pre} and shape were significant differences between metastases and LPAs in both the training and testing datasets (Table I; P<0.05).

Radiomics feature extraction, selection and Radscore construction. A total of 1,316 quantitative features were extracted from the plain CT images. The inter-observer ICC of the radiomics features was <0.5, 0.5-0.79 and ≥ 0.8 for 2, 6 and 92%, respectively, indicating that the reproducibility of feature extraction was deemed satisfactory. Based on the training dataset, 13 meaningful features were selected by LASSO (Fig. 3). Next, 9 features with high collinearity were deleted and 4 potential predictors remained to calculate the Radscore for each patient using the following formula: Radscore =1/[1+e^(82.3458+13.8774x origial_shape_Flatness+ 87.0981xwaveletLLH_glcm_Idn-0.0015xwaveletLLH_gldm_ DependenceNonUniformity-0.0301xwaveletLLL_firstorder_ Maximum)]. Patients with LPAs had relatively lower Radscores in both the training and testing datasets (Table I; P<0.05).

Validation of Radscore and the performance of significant clinical and imaging features. The Radscores for patients in the two cohorts were shown in Fig. 4A and B. The Radscore yielded an AUC of 0.920 [95% confidence interval (CI), 0.879-0.962] with a sensitivity, specificity and accuracy of 0.788 (95% CI, 0.689-0.887), 0.901 (95% CI, 0.832-0.971) and 0.847 (95% CI, 0.845-0.849) in the training dataset, respectively. An AUC of 0.888 (95% CI, 0.808-0.968) with a sensitivity, specificity and accuracy of 0.750 (95% CI, 0.590-0.910), 0.871 (95% CI, 0.753-0.989) and 0.814 (95% CI, 0.809-0.819) was achieved in the testing dataset, respectively (Fig. 4C and D). The Radscore showed the highest differential diagnostic performance compared with significant clinical-imaging features. The cut-off values for age, CT_{pre} and Rad-score were 60.5 years, 28.5 HU and 0.567, respectively (Table II).

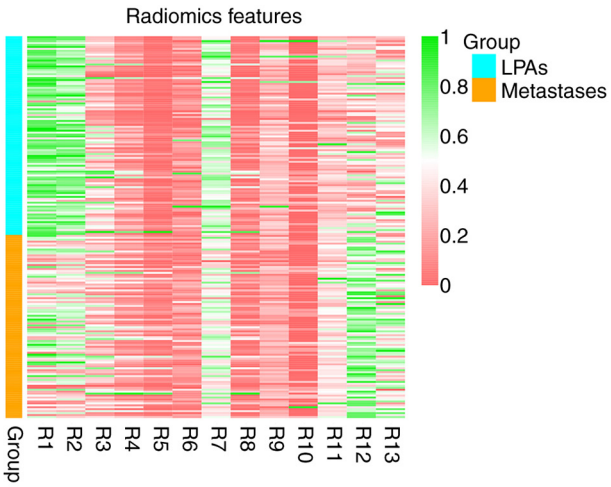

Figure 3. A total of 13 radiomics features of all the patients. LPAs, lipid-poor adenomas.

Validation of the clinical-imaging-radiomic model and nomogram. A total of four variables including sex, age, CT_{pre} and Radscore selected by multivariate logistic regression were independent factors for distinguishing between metastases and LPAs in patients with lung cancer. AIs in male patients [(Odds ratio, OR), 5.380 (1.267-22.850); P=0.024] with age >60.5 years [OR, 1.074 (0.998-1.156); P=0.057], CT_{pre} >28.5 HU [OR, 1.179 (1.078-1.289); P<0.001] and Radscore >0.567 [OR, 473.911 (41.943-5354.651); P<0.001] tended to have metastases.

The clinical-imaging-radiomic model provided an AUC of 0.968 in the training dataset and 0.915 in the testing dataset (Fig. 5A and B). Meanwhile, the AUCs of the clinical-imaging-radiomic model were significantly higher than the clinical-imaging model (details of the clinical-imaging model are found in Fig. S1) in both training and testing cohorts (Table III). The nomogram revealed that >115.33 could be considered lung cancer metastases, with an AUC of 0.953, a sensitivity of 92.6%, a specificity of 86.3% and an accuracy of 89.3% in the training dataset. The AUC, sensitivity, specificity and accuracy of the nomogram was 0.850, 89.3%, 80.6 and 84.7% in the testing dataset when using 115.33 as the cut-off value (Fig. 5C-E). Favourable calibration curves were shown in both the training (P=0.940) and testing datasets (P=0.094; Fig. 5F and G).

Clinical application value according to DCA. Compared with the clinical-imaging model (details of models in Fig. S1) and the Radscore, the DCA of the nomogram had the highest clinical net benefit at almost all the threshold probabilities, showing that the clinical-imaging-radiomic nomogram is a potential tool to effectively predict metastases in patients with lung cancer with small hyperattenuating AIs (Fig. 6).

Table II. The optimal cut-off values of individual variables in the training cohort by receiver operating characteristic analysis.

Variables	Cut-off	Area under the curve	Sensitivity	Specificity	PPV	NPV
Sex	-	0.668 (0.590-0.745)	79.8%	57.8%	62.5%	71.9%
Age	60.5	0.655 (0.563-0.747)	65.2%	67.6%	65.2%	67.6%
CT-pre	28.5	0.864 (0.805-0.924)	93.9%	67.6%	72.9%	92.3%
Shape	-	0.577 (0.526-0.628)	18.2%	97.2%	85.7%	56.1%
Rad-score	0.567	0.920 (0.879-0.962)	78.8%	90.1%	88.1%	82.0%

PPV, positive predictive value; NPV, negative predictive value.

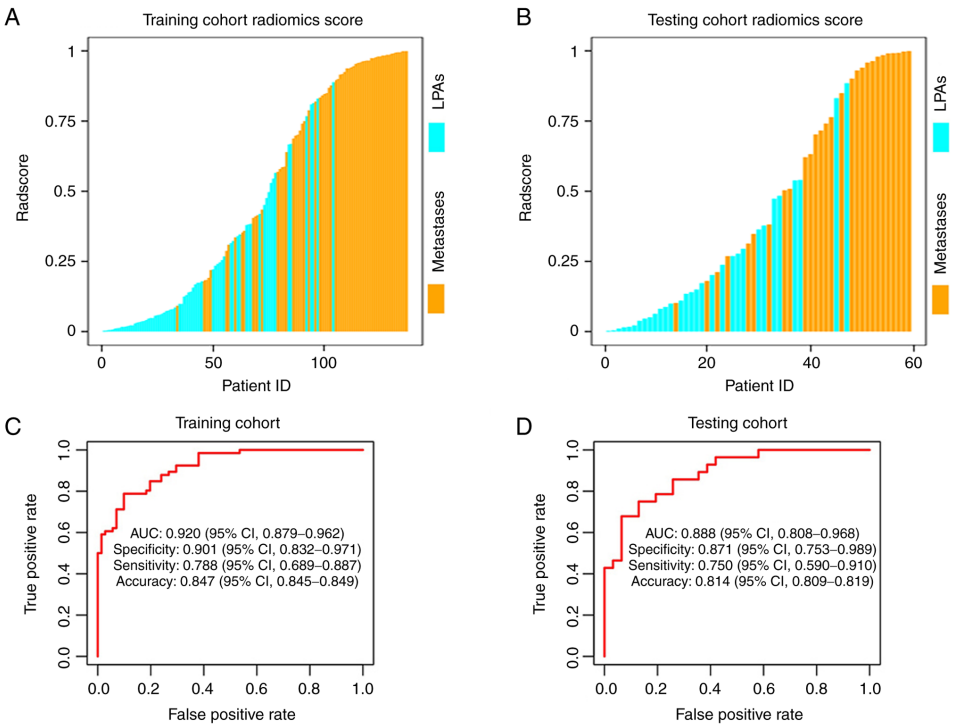

Figure 4. Sorted Radscore for patients in the (A) training cohort and (B) in the testing cohort. The Receiver operating characteristic curve of the Radscore in the (C) training cohort and in the (D) testing cohort. LPAs, lipid-poor adenomas.

Discussion

The present study aimed to settle a real diagnostic conundrum for clinicians and radiologists. Most patients with lung cancer present with adrenal metastases at the time of diagnosis and an adrenal mass may be the only sign of cancer dissemination (28). Correctly differentiating metastases from LPAs is pivotal for optimal treatment. While in clinical practice, small unilateral AIs with CT_{pre} ≥10 HU are usually discovered in patients with lung cancer undergoing routine non-contrast chest or abdominal CT scans. Unfortunately, most patients currently need to go for enhanced CT due to the difficulty in differentiating LPAs from metastases with initial plain CT (7-9). The present study was confined to initial plain CT on account that the aim was to determine whether the analysis based on initial plain CT images alone would be sufficient to make a satisfactory differential diagnosis. If the distinction was valid, it would help avoid the additional examinations and risks associated with contrast media.

Radiomics may be an important predictor for differential diagnosis in tumors and the application of Radiomics has been increasing in adrenal lesions (29,30). Yi *et al* (29) discovered that the radiomic nomograms by incorporating clinical risk factors and Radscore based on enhanced and unenhanced CT images could effectively differentiate lipid-poor adenoma from subclinical pheochromocytoma, with favourable specificity, sensitivity and accuracy. He *et al* (30) concluded that the radiomic nomogram based on pre-enhanced CT by integrating the Radscore and traditional clinical factors helped to effectively identify aldosterone-producing adenoma. To the best of our knowledge, few previous studies have determined whether a clinical-imaging-radiomic nomogram could be used to differentiate LPAs from metastases based on initial plain CT images in patients with lung cancer and with small unilateral AIs. Previous studies concerning adrenal metastases or LPAs have proved radiomics could provide some promising results. However, these findings have some limitations including small sample sizes, non-comprehensive

Table III. Comparison of the performance of the Radscore, clinical-imaging model, and clinical-imaging-radiomic model in both training and testing cohorts.

	Training cohort			Testing cohort		
Model	AUC	Z statistic	P-value	AUC	Z statistic	P-value
Clinical-imaging-radiomic model vs. clinical-imaging model	0.968 vs. 0.896	3.098	0.002	0.915 vs. 0.790	2.733	0.006
Clinical-imaging-radiomic model vs. Radscore	0.968 vs. 0.920	2.892	0.004	0.915 vs. 0.888	0.782	0.434
Clinical-imaging model vs. Radscore	0.896 vs. 0.920	0.726	0.468	0.790 vs. 0.888	1.393	0.164

AUC, area under the curve.

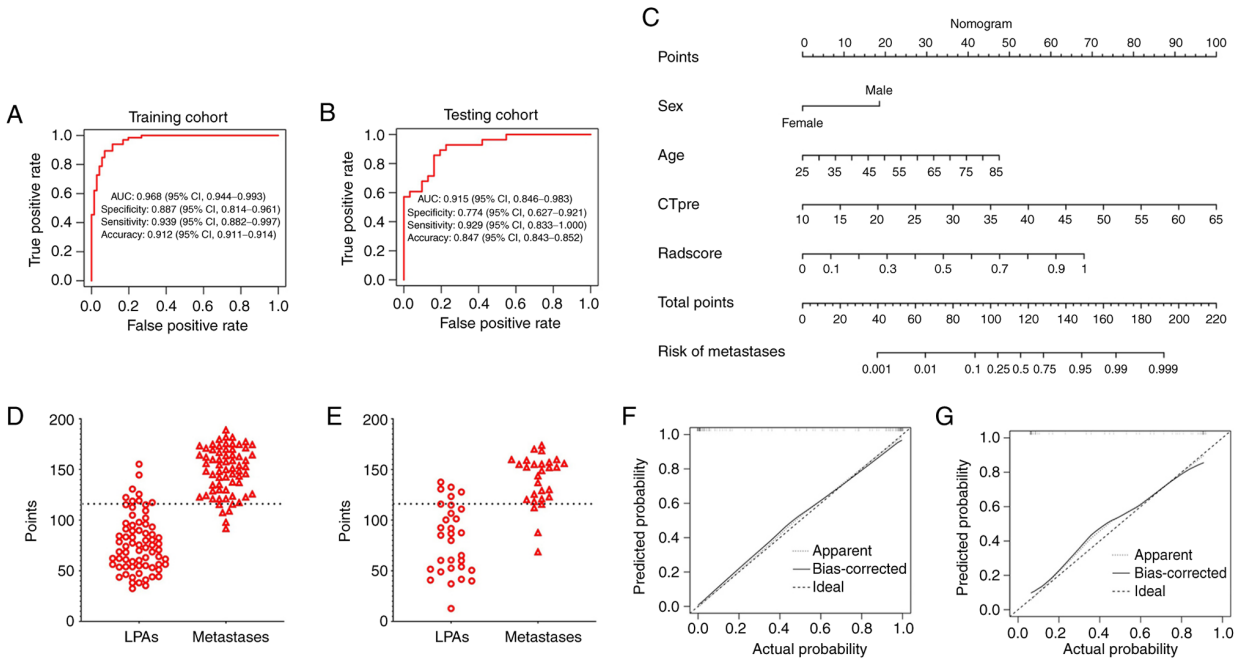

Figure 5. The receiver operating characteristic curve of the clinical-imaging-radiomic model in (A) the training cohort and in (B) the testing cohort. (C) The clinical-imaging-radiomic nomogram. (D and E) The difference in points between lipid-poor adenomas and metastases was apparent in the training cohort and in the testing cohort, and the dashed lines represented the cut-off value (115.3) of nomogram points. (F and G) Calibration curve of the clinical-imaging-radiomic nomogram in the training cohort and in the testing cohort. CT_{pre}, pre-enhanced CT value.

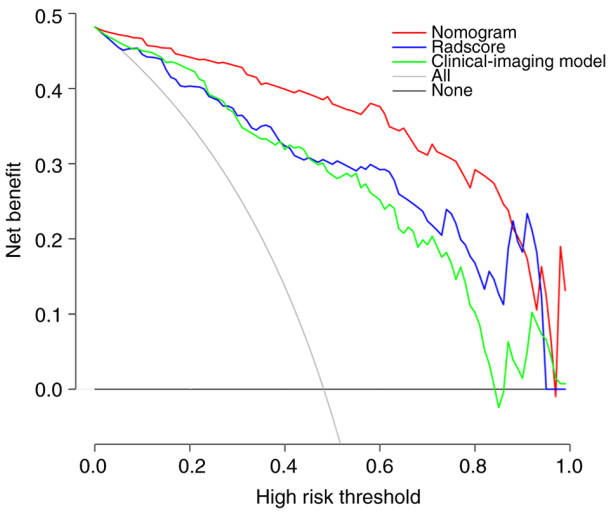

Figure 6. Decision curve analysis for the Radscore, clinical-imaging model and nomogram model.

analysis (no combination of clinical, radiological features and radiomics features), involving different primary malignant tumors or different adrenal malignant tumors, and no studies have introduced Radscore (4,31,32). For example, Ho *et al* (31) revealed that the contrast-enhanced CT texture features achieved a mean AUC of 0.800, indicating the potential ability for distinguishing between benign and malignant lesions. Yet, the malignant lesions included not only metastases but also two cases of adrenal cortical carcinomas, and the study suffered from a small sample size (20 patients). In addition, Ho *et al* (31) did not discuss primary malignant tumors. Furthermore, although Andersen *et al* (4) proved certain texture parameters could statistically differentiate benign adrenal masses from metastases in patients with a history of lung cancer and constructed a diagnostic model, the AUC (0.73), sensitivity (58%), accuracy (68%) and specificity (77%) were relatively low.

As a part of a growing number of studies using Radscore, the present study established a Radscore using 4 radiomics features on unenhanced CT, and the best cut-off value of 0.567 afforded a specificity of 90.1% and a sensitivity of 78.8% for identifying adrenal metastases in the testing cohort. In addition, the Radscore had favourable predictive performance for adrenal metastases with an AUC of 0.888 and OR of 473.911, which demonstrated that the Radscore could be a useful stand-alone factor for identifying metastases from LPAs in patients with lung cancer.

Sex and age, as clinical-imaging risk factors, were included in the predictive model for distinguishing LPAs from lung cancer metastases in the present study. It was revealed that male patients aged >60.5 years were associated with a higher likelihood of being diagnosed with lung cancer metastases. This observation may be attributed to the specific selection of lung cancer (33). Additionally, CT_{pre} was another important feature for identifying metastases of lung cancer. Metastases exhibited significantly higher plaint CT attenuation compared with LPAs, with a cut-off value exceeding 28.5 HU and an OR of 1.179. This finding aligns with previous research by Ho *et al* (31), who revealed the statistical significance of unenhanced CT attenuation in distinguishing benign from malignant adrenal masses. Homogeneity, shape and border revealed no statistical significance in the present study, inconsistent with Moawad *et al* (34) and Ho *et al* (31). It is likely that the small size of metastases (≤4 cm) used in the present study reflects the early stages of cancer, without neo-angiogenesis or necrosis, thus they demonstrated approximately the same homogeneous, uniform and fine with LPAs from traditional imaging assessment (35,36).

The present study developed a clinical-imaging-radiomic nomogram by integrating the Radscore, sex, age and CT_{pre} based on pre-enhanced CT for identifying metastases from LPAs with a large study cohort, and the diagnostic performance of which was further improved (AUC=0.915). The present study demonstrated that the clinical-imaging-radiomic nomogram based on initial plain CT images is a potential tool to predict metastases successfully before surgery, which could enable individualized treatment strategies for each patient with lung cancer. The promising results of the present study may have important clinical applications including that additional examinations may no longer be required. Compared with enhanced CT, PET/CT or MRI, the plain CT is easier to obtain, is less time-consuming, produces reliable image quality and is cheaper. Therefore, the findings of the present study can be quickly applied to clinical practice.

In conclusion, the novel points of the present study contain three key aspects: i) The focus on a specific research population, namely patients with small unilateral AIs, as opposed to previous studies which included all AIs regardless of size or laterality (4,31,32); ii) the differentiation between adrenal metastases and LPAs based solely on plain CT images with a large sample size, in contrast to most previous studies that utilized enhanced CT images with smaller sample sizes and generally distinguished between benign [(including adrenal adenoma and other benign lesions (for example, oncocytoma and ganglioneuroma)] and malignant (including adrenal metastases and adrenocortical carcinomas) adrenal tumors (4,31,34); and iii) an improved AUC value of 0.915 for the model developed in the present study compared with previous studies (AUC=0.730-0.850), indicating the current model has superior predictive performance (4,31,34).

The present study has several noteworthy limitations. Firstly, the single-centre and retrospective nature of the study may introduce population bias, which could limit the generalizability of the findings. Secondly, a subset of patients did not have histological confirmation in accordance with the inclusion criteria of the study, potentially leading to diagnostic uncertainty in these cases. Thirdly, the present research lacked external validation of the nomogram. To enhance the robustness and reliability of the present findings, further research should prioritize validation on a larger scale, potentially involving multiple centres.

In conclusion, the clinical-imaging-radiomic nomogram built by integrating the Radscore and traditional clinical-imaging risk factors helped to accurately identify metastases in patients with lung cancer with small hyperattenuating AIs.

Acknowledgements

Not applicable.

Funding

No funding was received.

Availability of data and materials

The data generated in the present study are not publicly available due to patient privacy purposes but may be requested from the corresponding author.

Authors' contributions

JL, YL, LC, WX and HC designed the study. LC, HY, DY, HW, YY and LZ collected, analyzed and interpreted the data. LC, HY and DY wrote the original draft of the manuscript. WX and HC reviewed the manuscript. LC and HW confirm the authenticity of all the raw data. All authors contributed to the article, and read and approved the final version of the manuscript.

Ethics approval and consent to participate

The present study was approved (approval no. RMYY-LLKS-2023202) by the Medical Ethics Committee of Tangshan People's Hospital (Tangshan, China). Written informed consent was obtained from each patient included and the present study was performed in accordance with the 1964 Helsinki Declaration and its later amendments or comparable ethical standards.

Patient consent for publication

The patients provided written informed consent for publication.

Competing interests

The authors declare that they have no competing interests.

References

1. Barzon L, Sonino N, Fallo F, Palu G and Boscaro M: Prevalence and natural history of adrenal incidentalomas. Eur J Endocrinol 149: 273-285, 2003.
2. Song JH, Chaudhry FS and Mayo-Smith WW: The incidental adrenal mass on CT: Prevalence of adrenal disease in 1,049 consecutive adrenal masses in patients with no known malignancy. AJR Am J Roentgenol 190: 1163-1168, 2008.
3. Fassnacht M, Arlt W, Bancos I, Dralle H, Newell-Price J, Sahdev A, Tabarin A, Terzolo M, Tsagarakis S and Dekkers OM: Management of adrenal incidentalomas: European society of endocrinology clinical practice guideline in collaboration with the european network for the study of adrenal tumors. Eur J Endocrinol 175: G1-G34, 2016.
4. Andersen MB, Bodtger U, Andersen IR, Thorup KS, Ganeshan B and Rasmussen F: Metastases or benign adrenal lesions in patients with histopathological verification of lung cancer: Can CT texture analysis distinguish? Eur J Radiol 138: 109664, 2021.
5. Terzolo M, Stigliano A, Chiodini I, Loli P, Furlani L, Arnaldi G, Reimondo G, Pia A, Toscano V, Zini M, *et al*: AME position statement on adrenal incidentaloma. Eur J Endocrinol 164: 851-870, 2011.
6. Gaujoux S, Mihai R and Joint working group of ESES and ENSAT: European society of endocrine surgeons (ESES) and european network for the study of adrenal tumours (ENSAT) recommendations for the surgical management of adrenocortical carcinoma. Br J Surg 104: 358-376, 2017.
7. Young WF Jr.: Clinical practice. The incidentally discovered adrenal mass. N Engl J Med 356: 601-610, 2007.
8. Ilias I, Sahdev A, Reznek RH, Grossman AB and Pacak K: The optimal imaging of adrenal tumours: A comparison of different methods. Endocr Relat Cancer 14: 587-599, 2007.
9. Zeiger MA, Siegelman SS and Hamrahian AH: Medical and surgical evaluation and treatment of adrenal incidentalomas. J Clin Endocrinol Metab 96: 2004-2015, 2011.
10. Mayo-Smith WW, Song JH, Boland GL, Francis IR, Israel GM, Mazzaglia PJ, Berland LL and Pandharipande PV: Management of incidental adrenal masses: A white paper of the ACR incidental findings committee. J Am Coll Radiol 14: 1038-1044, 2017.
11. Bednarczuk T, Bolanowski M, Sworczak K, Górnicka B, Cieszanowski A, Otto M, Ambroziak U, Pachucki J, Kubicka E, Babińska A, *et al*: Adrenal incidentaloma in adults-management recommendations by the Polish society of endocrinology. Endokrynol Pol 67: 234-258, 2016.
12. Pandharipande PV, Herts BR, Gore RM, Mayo-Smith WW, Harvey HB, Megibow AJ and Berland LL: Rethinking normal: Benefits and risks of not reporting harmless incidental findings. J Am Coll Radiol 13: 764-767, 2016.
13. Fujiyoshi F, Nakajo M, Fukukura Y and Tsuchimochi S: Characterization of adrenal tumors by chemical shift fast low-angle shot MR imaging: Comparison of four methods of quantitative evaluation. AJR Am J Roentgenol 180: 1649-1657, 2003.
14. Guerin C, Pattou F, Brunaud L, Lifante JC, Mirallié E, Haissaguerre M, Huglo D, Olivier P, Houzard C, Ansquer C, *et al*: Performance of 18F-FDG PET/CT in the characterization of adrenal masses in noncancer patients: A prospective study. J Clin Endocrinol Metab 102: 2465-2472, 2017.
15. Caoili EM, Korobkin M, Francis IR, Cohan RH, Platt JF, Dunnick NR and Raghupathi KI: Adrenal masses: Characterization with combined unenhanced and delayed enhanced CT. Radiology 222: 629-633, 2002.
16. Haider MA, Ghai S, Jhaveri K and Lockwood G: Chemical shift MR imaging of hyperattenuating (>10 HU) adrenal masses: does it still have a role? Radiology 231: 711-716, 2004.
17. Koo HJ, Choi HJ, Kim HJ, Kim SO and Cho KS: The value of 15-minute delayed contrast-enhanced CT to differentiate hyperattenuating adrenal masses compared with chemical shift MR imaging. Eur Radiol 24: 1410-1420, 2014.
18. Akkus G, Guney IB, Ok F, Evran M, Izol V, Erdogan S, Bayazit Y, Sert M and Tetiker T: Diagnostic efficacy of 18F-FDG PET/CT in patients with adrenal incidentaloma. Endocr Connect 8: 838-845, 2019.
19. Kassirer JP: Our stubborn quest for diagnostic certainty. A cause of excessive testing. N Engl J Med 320: 1489-1491, 1989.
20. Lambin P, Leijenaar RTH, Deist TM, Peerlings J, de Jong EEC, van Timmeren J, Sanduleanu S, Larue R, Even AJG, Jochems A, *et al*: Radiomics: the bridge between medical imaging and personalized medicine. Nat Rev Clin Oncol 14: 749-762, 2017.
21. Yang C, Jiang Z, Cheng T, Zhou R, Wang G, Jing D, Bo L, Huang P, Wang J, Zhang D, *et al*: Radiomics for predicting response of neoadjuvant chemotherapy in nasopharyngeal carcinoma: A systematic review and meta-analysis. Front Oncol 12: 893103, 2022.
22. Gillies RJ, Kinahan PE and Hricak H: Radiomics: Images are more than pictures, they are data. Radiology 278: 563-577, 2016.
23. Zhang Z, Yang J, Ho A, Jiang W, Logan J, Wang X, Brown PD, McGovern SL, Guha-Thakurta N, Ferguson SD, *et al*: Correction to: A predictive model for distinguishing radiation necrosis from tumour progression after gamma knife radiosurgery based on radiomic features from MR images. Eur Radiol 28: 3570-3571, 2018.
24. Nishino M, Jagannathan JP, Ramaiya NH and Van den Abbeele AD: Revised RECIST guideline version 1.1: What oncologists want to know and what radiologists need to know. AJR Am J Roentgenol 195: 281-289, 2010.
25. Lee HY, Oh YL and Park SY: Hyperattenuating adrenal lesions in lung cancer: Biphasic CT with unenhanced and 1-min enhanced images reliably predicts benign lesions. Eur Radiol 31: 5948-5958, 2021.
26. Liu H, Guan X, Xu B, Zeng F, Chen C, Yin HL, Yi X, Peng Y and Chen BT: Computed tomography-based machine learning differentiates adrenal pheochromocytoma from lipid-poor adenoma. Front Endocrinol (Lausanne) 13: 833413, 2022.
27. Zhang GM, Shi B, Sun H, Jin ZY and Xue HD: Differentiating pheochromocytoma from lipid-poor adrenocortical adenoma by CT texture analysis: feasibility study. Abdom Radiol (NY) 42: 2305-2313, 2017.
28. Ettinghausen SE and Burt ME: Prospective evaluation of unilateral adrenal masses in patients with operable non-small-cell lung cancer. J Clin Oncol 9: 1462-1466, 1991.
29. Yi X, Guan X, Zhang Y, Liu L, Long X, Yin H, Wang Z, Li X, Liao W, Chen BT and Zee C: Radiomics improves efficiency for differentiating subclinical pheochromocytoma from lipid-poor adenoma: A predictive, preventive and personalized medical approach in adrenal incidentalomas. EPMA J 9: 421-429, 2018.
30. He K, Zhang ZT, Wang ZH, Wang Y, Wang YX, Zhang HZ, Dong YF and Xiao XL: A clinical-radiomic nomogram based on unenhanced computed tomography for predicting the risk of aldosterone-producing adenoma. Front Oncol 11: 634879, 2021.
31. Ho LM, Samei E, Mazurowski MA, Zheng Y, Allen BC, Nelson RC and Marin D: Can texture analysis be used to distinguish benign from malignant adrenal nodules on unenhanced CT, contrast-enhanced CT, or in-phase and opposed-phase MRI? AJR Am J Roentgenol 212: 554-561, 2019.
32. Tu W, Verma R, Krishna S, McInnes MDF, Flood TA and Schieda N: Can adrenal adenomas be differentiated from adrenal metastases at single-phase contrast-enhanced CT? AJR Am J Roentgenol 211: 1044-1050, 2018.
33. de Groot P and Munden RF: Lung cancer epidemiology, risk factors, and prevention. Radiol Clin North Am 50: 863-876, 2012.
34. Moawad AW, Ahmed A, Fuentes DT, Hazle JD, Habra MA and Elsayes KM: Machine learning-based texture analysis for differentiation of radiologically indeterminate small adrenal tumors on adrenal protocol CT scans. Abdom Radiol (NY) 46: 4853-4863, 2021.
35. You X, Sun X, Yang C and Fang Y: CT diagnosis and differentiation of benign and malignant varieties of solitary fibrous tumor of the pleura. Medicine (Baltimore) 96: e9058, 2017.
36. Ganeshan B, Goh V, Mandeville HC, Ng QS, Hoskin PJ and Miles KA: Non-small cell lung cancer: Histopathologic correlates for texture parameters at CT. Radiology 266: 326-336, 2013.